

Journal of Computational and Applied Research in Mechanical Engineering

jcarme.sru.ac.ir



Research paper

Numerical and experimental study of heatsink cooling of brushless direct current electric motors

I W. Y. Arta^a, A. Ghurri ^{a,*}, I N. S. Winaya^a and I K. Warjaya^b

^aDepartment of Mechanical Engineering, Udayana University, Bali, 80361, Indonesia ^bDepartment of Mechanical Engineering, Institut Teknologi Sepuluh Nopember, Surabaya, Jawa Timur, 60111, Indonesia

Article info: Article history: Received: 00/00/0000 Accepted: 00/00/0018 Revised: 00/00/0000 00/00/0000 Online: **Keywords:** Heatsink, Cooling, Motor, Temperature. *Corresponding author:

1. Introduction

a ghurri@unud.ac.id

Vehicles typically rely on fossil fuels as their primary energy source for starting engines. However, fossil fuels are non-renewable and are depleting at an increasing rate, leading to concerns about an energy crisis. Additionally, motorized vehicles are known to produce exhaust gases that are harmful to human health and contribute to global warming. According to the emission inventory from 2021 to 2022, it was found that 70% of emissions in urban areas are generated by motorized vehicles. This highlights

Abstract

The cooling system used in brushless direct current motors employs an aircooling mechanism with fins on the motor heatsink. The optimal performance of brushless direct current motor cooling is not yet fully understood, necessitating an analysis of the cooling process. This study employs two methods, experimental and simulation, to investigate cooling efficiency. The results indicate that the temperatures of the winding and heatsink increase with the electric motor's rotation speed. The highest temperature recorded with a thermocouple was 94°C at 2000rpm. Validation of the simulation results against the experimental results showed a 2% deviation, indicating their validity. Based on these findings, three new heatsink designs, namely modif 1, modif 2, and modif 3, were developed. Simulation results revealed that modif 3, a combination of axial and radial heatsink shapes, exhibited the most effective temperature transfer. Therefore, it can be inferred that higher motor rotation speeds can lead to increased motor heat. The study concludes that a combination heatsink design is capable of reducing temperatures in brushless direct current motors, as demonstrated through CFD simulations on electric motor prototypes.

> the significant impact that these vehicles have on air quality and the environment [1]. Therefore, it is necessary to find alternative energy sources are more environmentally friendly, abundant, and easy to access [2]. Electric vehicles are being developed as an alternative to fuel-powered vehicles environmental impact and dependence on fossil fuels. Accelerating the adoption of battery-based electric vehicles is essential to improve energy efficiency, energy security, and energy conservation in the transportation sector [3].

Development and innovation to support electric vehicle infrastructure in Indonesia should be encouraged, involving all stakeholders. Electric vehicles are considered emission-free compared to fossil fuel vehicles, as they do not have a combustion component and are powered by an electric motor supplied by a battery. There are several types of electric motors, with Brushless Direct Current (BLDC) motors being a common type. BLDC motors operate based on the attractive force between magnets with the same poles, which causes the motor to rotate. It's important to note that the higher the engine speed, the greater the change in cooling water temperature [4]. In construction, the BLDC motor has fixed poles because the BLDC rotor contains permanent magnets, while the BLDC stator consists of wire windings. This design allows the magnetic poles to change depending on the current polarity of the stator winding, which is controlled by the controller. However, the continuous flow of current in the stator winding generates heat, which can affect the magnets in the rotor.

Magnetic and magnetic field strength decrease with increasing temperature [5]. So, from this research, the performance of electric motors can be affected by the temperature of the magnets used in the motor. As temperature increases, the performance of the magnets can decrease, leading to changes in the motor's power and torque output. In your example, you mentioned that an electric motor operating at 125°C requires a greater current to achieve the same torque as a motor operating at 25°C. This is because the magnetic properties of the materials in the motor, including the magnets, change with temperature. As a result, the motor's ability to produce torque can vary depending on its operating temperature [6]. This shows that changes in temperature increase can reduce the performance of the electric motor. So, to maintain the performance of BLDC motors on electric motor prototypes, it is necessary to carry out appropriate cooling management for electric motors.

The electric motor prototype is an electric motor made at Poltrada Bali. The cooling used in BLDC motors uses an air-cooling system that uses fins on the motor heatsink. The optimal performance of the BLDC motor cooling is not yet known, so it is necessary to analyze the motor cooling. Heatsink is a component of an electronic device whose function is to transfer heat obtained from parts of electronic or mechanical devices to a fluid medium in the form of air or liquid cooling, so that the heat can be reduced in these components and component temperatures will be maintained at optimal temperatures [7]. Based on the problems above, it is necessary to design or plan cooling according to the capacity of the BLDC motor This process, which used. consists experiments and simulations, will be carried out in this work using a BLDC motor type. Experimental research was conducted to obtain data as initial conditions during the simulation. The simulation uses Ansys Fluent software to determine the temperature distribution on the heatsink and to determine the temperature of the electric motor. The heatsink in question is the outer cover of the electric motor, which transfers the heat generated by the electric motor through air cooling. From the simulation results obtained, validation will be carried out using experimental data obtained previously during the experimental testing of the electric motor prototype at Poltrada Bali.

Research on optimizing heatsink geometry for vehicle **BLDC** motor electric using computational fluid dynamics (CFD) with 3D CFD simulations carried out on fan-cooled BLDC motors to identify the critical temperature of the motor and to determine the cooling performance of the motor. The results showed that the highest temperature on the winding and hot temperatures can be reduced up to 15% by a suitable housing. These results explain that CFD simulation can be used effectively to optimize the cooling performance of electric motors [8]. Research on the new cooling system design of BLDC motor for electric vehicle using CFD modeling explains that analyzing the cooling of a 1.2 kW BLDC motor by varying the shape of the BLDC model can produce a lower temperature distribution compared to the initial model. This research uses Ansys ICEM CFD with tetrahedral meshing type and boundary conditions, including inlet velocity, outlet

pressure as a pressure boundary condition, which is set as atmospheric pressure [9].

Research on "numerical and experimental investigation of heat flow in permanent magnet BLDC hub motor" shows that the modeling of heat transfer by convection at the hub motor using the thermal Lumped Parameter (LP) model is validated with finite element (FE) and experimental data, while CFD is used for modeling flow on internal and external hub motors. Thus, hub motor optimization studies carried out using simulation methods can increase heat transfer [10]. Research on "heatimprovements in an axial-flux permanent-magnet synchronous machine" describes the CFD method used to analyze the temperature distribution of the motor. The results show that copper accelerates heat transfer significantly. It can also be concluded that the pot of the axial engine stator can reduce the motor temperature in a more efficient way [11]. Research on "parametric study of thermal performance of BMW I3" shows that research uses CFD simulations with 3D models to simulate thermal performance on permanent magnet synchronous motors (PMSM). Sensitivity analyses have been carried out on various convection heat transfer coefficients of the stator. Numerical results show that the thermal conductivity of the winding liner and the forced heat transfer coefficient have a significant effect on PMSM thermal [12].

The research on "thermal analysis of a gramme ring winding high speed permanent magnet motor for pulsed alternator using CFD" explains that this study investigated the cooling problem of a 300-kW motor using a water jacket and forced air cooling at a speed of 12,000 rpm. The results showed that the wind resistance that occurs in the ventilation ducts of the stator laminations and water jackets is the main problem. Improvement of the ventilation structure is calculated to reduce wind resistance. In addition, modifications to the water channels were also carried out to avoid the influence of a large interface gap on the water-cooling performance. With a suitable cooling structure, the motor temperature rise is reduced, and motor performance can be increased [13]. Research on "liquid cooling model axial BLDC motor"

explains that cooling temperature has a significant effect on motor power and efficiency. Lower temperatures result in higher motor power and efficiency. Liquid-cooled motors can produce a maximum power of up to 6 kW and an efficiency of up to 88%, while air-cooled motors only produce a maximum power of 3.5 kW and an efficiency of up to 55%. From these results, it can be concluded that proper motor cooling can increase efficiency by 33% [14]. Thus, the robustness of the scheme has increased interest among the CFD community. [15].

Research on "design and material optimization of cooling fins in electric motors" explains that to overcome the problem of heat transfer with the design of motor fins, modeling is carried out in 3D modeling software (DSS-Solidwork) and analyzed by Ansys_2016 for its heat transfer properties. From the results obtained, it is clear that Al-6061(T6) is the best material among the 3 materials, namely Al-6061(T6), brass, and cast iron [16]. Radiation heat transfer is not taken into account in this study because heat transfer occurs without any intermediary substances. Radiation can also usually be accompanied by light.

2. BLDC motor specifications

The components that make up the BLDC electric motor consist of several parts, shown in Fig. 1. The heatsink and cover casing, made of Al-6061(T6), are the outermost parts of the electric motor and also serve as a protector of the motor. The stator has 12 poles made of electric steel material; each pole is given a wire coil using 0.8 mm diameter enameled wire arranged in parallel.

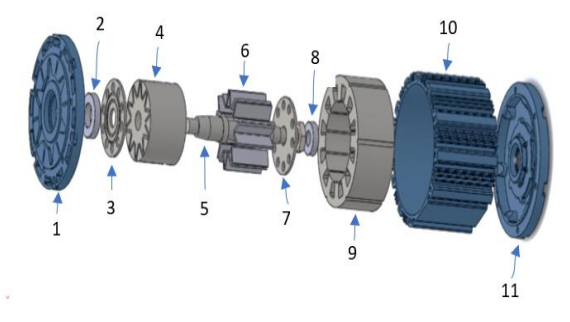


Fig. 1. Motor specification; 1. Close the top casing, 2. Upper bearing, 3. Top stopper magnet, 4. Disc rotors, 5. As a mover, 6. Magnets, 7. Magnet stopper bottom, 8. Bottom bearing, 9. Winding, 10. Heatsinks, and 11. Close the bottom casing.

Furthermore, the rotor consists of a shaft, a magnetic housing, and magnets. Magnets are as many as 20 pcs. Overall, the BLDC motor can be seen in the following figure.

3. Heat generation in BLDC motors

Electric motors can have disadvantages which can be grouped as follows:

3.1. Resistive losses

Resistive losses are generally the main component of power losses in permanent magnet brushless direct current (PMBLDC) motors and can be calculated using Eq. (1):

$$P_r = \mathrm{m} \, l_{ph}^2 R_{ph} \tag{1}$$

where:

Pr: resistive losses m: number of phases l^2_{ph} : current phase R_{ph} : resistance

Resistance varies with temperature and can be calculated from resistance at other temperatures as follows.

3.2. Loss per unit mass due to hysteresis (Ph)

The stator core is made of silicon steel insulated laminates. Therefore, variations in magnetic flux from the rotation of the magnets produce eddy losses and hysteresis losses in the lamination. The loss is estimated at the stator yoke gear to be caused independently, as the variation of the field inside is different. The mass loss per unit due to hysteresis, the eddy current in the stator yoke, and the eddy current in the stator tooth are calculated using Eq. (2) as:

$$P_h = K_h f^a B m^\beta \tag{2}$$

where:

Ph: loss per unit mass due to hysteresis

Kh: hysteresis loss constant f: frequency of flux variation Bm: peak flux density

K_e: excess eddy current loss constant

a: angle of lag

3.3. Losses eddy current pada stator voke (Pev)

The eddy current losses in the stator yoke can be calculated using Eq. (3):

$$P_{ey} = K_e \frac{8}{\pi} \frac{f^2 B m^2}{\beta_m} \pi r^2$$
 (3)

where:

P_{ey}: eddy current losses on the stator yoke

K_e: excess eddy current loss constant

f: frequency of flux variation

Bm: peak flux density

 βm : are tooth and pole width each in electrical

radians

r: polar coordinates

3.4. Losses eddy current pada stator toots (Pet)

The eddy current losses in the tooth stator can be calculated using Eq. (4):

$$P_{et} = K_e \frac{4}{\pi} \frac{f^2 B m^2}{a_{tt}} \left[2 - \frac{\pi - \beta_m}{a_{tt}} \right]' \tag{4}$$

where:

Pet: eddy current losses at stator toots

f: frequency of flux variation

Bm: peak flux density

Ke: excess eddy current loss constant

a: angle of lag

β: parameter characterizing the effect of slotting on the airgap flux density distribution

The graph of core loss to speed on the BLDC motor is shown in Fig. 2.

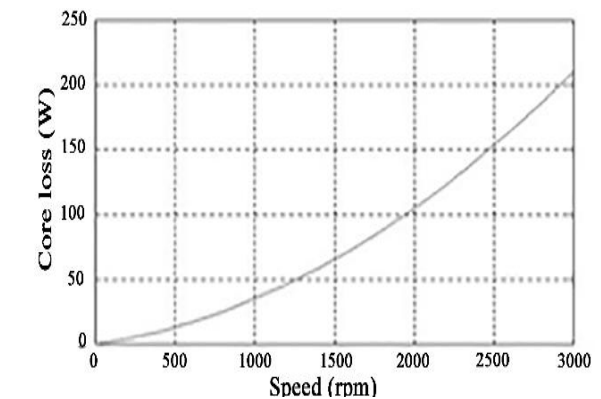


Fig. 2. Core loss in electric motors.

4. Methods

The concept of research conducted in this study involves experimental and simulation methods. Experimental research is carried out using the main variable, namely the rotation of the BLDC motor, with the dependent variable being the distribution of heat on the heatsink and the motor winding temperature. The winding motor temperature value is used as the initial condition for the simulation. The simulation results are used to investigate the temperature distribution on the BLDC motor heatsink. Simulation and experimental results compared and analyzed. Furthermore, the data is used as a basis for redesigning the heatsink. As a result, better temperature distribution and cooling performance are expected compared to the previous desig. In general, the concept of this research is shown in Fig. 3.

The first stage of experimental research involves data collection. The data to be obtained in the experimental research are power and torque. electric current, heat distribution on the heatsink, temperature. and motor winding temperature at the winding motor is measured using a thermocouple. The temperature value obtained is used as initial data to carry out the simulation. Simulation data are compared and validated using data previously obtained during experimental research. Both of these datasets can be used to analyze and create an optimal design for BLDC motor cooling. Experimental research data include: power and torque, electric current, heat distribution on the heatsink, and motor winding temperature with variations in the rpm of the electric motor.

CFD simulation results include heat distribution on the BLDC motor heatsinks, heat transfer, and heatsink redesign with the hope of better temperature distribution and cooling than before. The independent variable is BLDC motor speed (750, 1000, 1250, 1500, 1750, 2000 rpm). The dependent variables are temperatures on the motor heatsink, windings, electric current, power, and torque of the BLDC motor. The control variables are a 3000 W BLDC motor, room temperature, battery voltage, and controller.

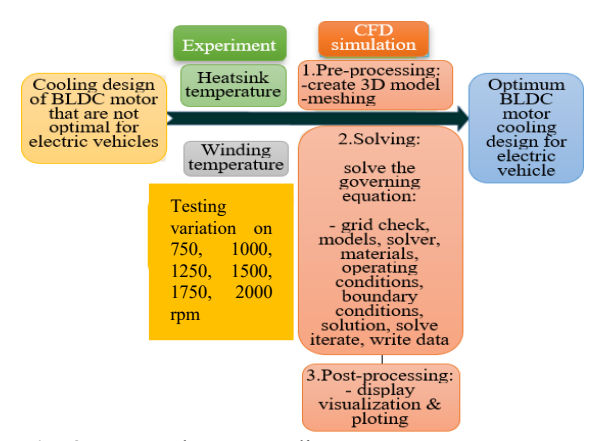


Fig. 3. Research concept diagram.

To carry out this research, several tools and materials need to be prepared, including the Ansys Fluent commercial software, BLDC motor, dyno test, thermal camera, and thermocouple.

The simulation method is carried out on Ansys Fluent software. The simulation method is used to determine the heat distribution and analyze the heat transfer that occurs in the heatsink. In general, the simulation method is carried out in 3 stages: pre-processing, completion, and post-processing. The novelty of the present research is the form of heatsink redesigned for BLDC motors. The data obtained can be used as a basis for reference to create new designs that are optimal for cooling electric motor prototypes.

5. Simulation results and measurements

There are 4 location points for the thermocouple sensor on the electric motor. The temperature distribution in the winding section is higher than the heatsink, as shown in Fig. 4.

The following is the installation of a thermocouple on an electric motor [17]. The testing phase using the thermocouple sensor is conducted according to the previous stage. Based on the measurement of the thermocouple sensor on the BLDC motor in Fig. 4, the results of the measurements using a thermocouple sensor are shown in Table 1.

CFD simulations are carried out for each test with simulated parameter settings. The simulation uses a poly-hexcore type mesh. The results of the poly-hexcore meshing type are shown in Fig. 5.

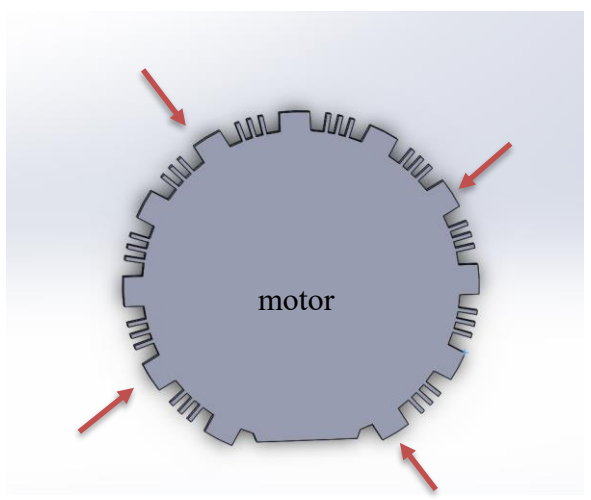


Fig. 4. Position of the thermocouple sensor.

Parameters from the results of meshing using poly-hexcore type meshing on the heatsink are 69119 cells, while the results of meshing the heatsink temperature to the environment using poly-hexcore are 2314550 cells. The maximum convergence of the simulation results is indicated by the cessation of iterations because the residuals of the numerical solutions have reached their maximum point or converged. Thus, in each simulated case, the convergence value varies depending on the problems being computed (Prasetvo et al. 2018). In this study, iterations are carried out until convergence. The convergence value of the residue generated by the standard motor heatsink simulation is Energy = 9.680e-07.

The value of each convergence of the residue generated by the heatsink temperature simulation with the environment is as follows:

- 1. Continuity = 6.7323e-06.
- 2. X velocity = 7.4051e-08.
- 3. Y velocity = 7.5270e-07.
- 4. Z velocity = 7.0562e-07.
- 5. Energy = 7.3607e-08.
- 6. k-omega= 5.3172e-06.

Table 1. Measurement results using a thermocouple.

RPM	Winding temperature (⁰ C)		
750	39		
1000	48		
1250	58		
1500	69		
1750	81		
2000	94		

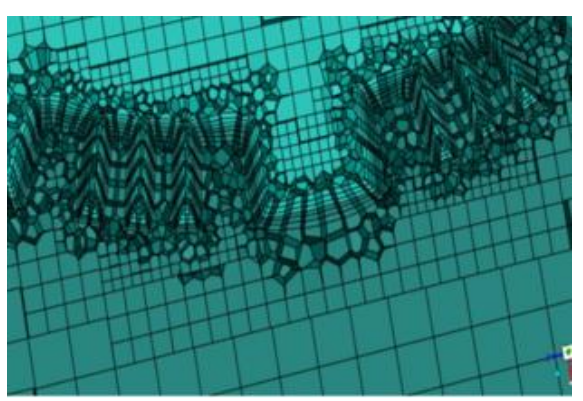


Fig. 5. Meshing results.

The maximum convergence value that the Ansys Fluent software can solve. The general convergence value targeted for CFD simulation cases using Ansys Fluent software is a minimum of 1.e-03 for each calculation variable [18, 19].

5.1. Heatsink motor CFD simulation results

The CFD heatsink simulation is carried out according to the data obtained during the experiment. The data is used as a reference for determining the temperature of the winding motor, namely 39°C, 48°C, 58°C, 69°C, 81°C, and 94°C. The standard motor heatsink simulation results are shown in Fig. 6.

The temperature value on the outside of the heatsink is 309.7°K or 36.5°C, with a temperature value of 39°C on the winding motor. The temperature value on the outside of the heatsink is 318.3°K or 45.1°C, with a temperature value of 48°C on the winding motor. The temperature value on the outside of the heatsink is 328.1°K or 55°C, with a temperature value of 58°C on the winding motor. The temperature value on the outside of the heatsink is 338.9°K or 65.7°C, with a temperature value of 69°C on the winding motor. The temperature value on the outside of the heatsink is 350.7°K or 77.5°C, with a temperature value of 81°C on the winding motor. The temperature value on the outside of the heatsink is 363.4°K or 90.2°C, with a temperature value of 94°C on the winding motor. The temperature drop is 4°C between the winding temperature and heatsink the temperature.

5.2. Thermal camera test results

In the experimental process, testing is also carried out using a thermal camera to determine the distribution of heat on the heatsink. The measurement results using a thermal camera are measured on the outer heatsink of the electric motor, which has the highest temperature. The data collection method can be shown in Fig. 7. The results obtained in testing using a thermal camera are shown in Table 2.

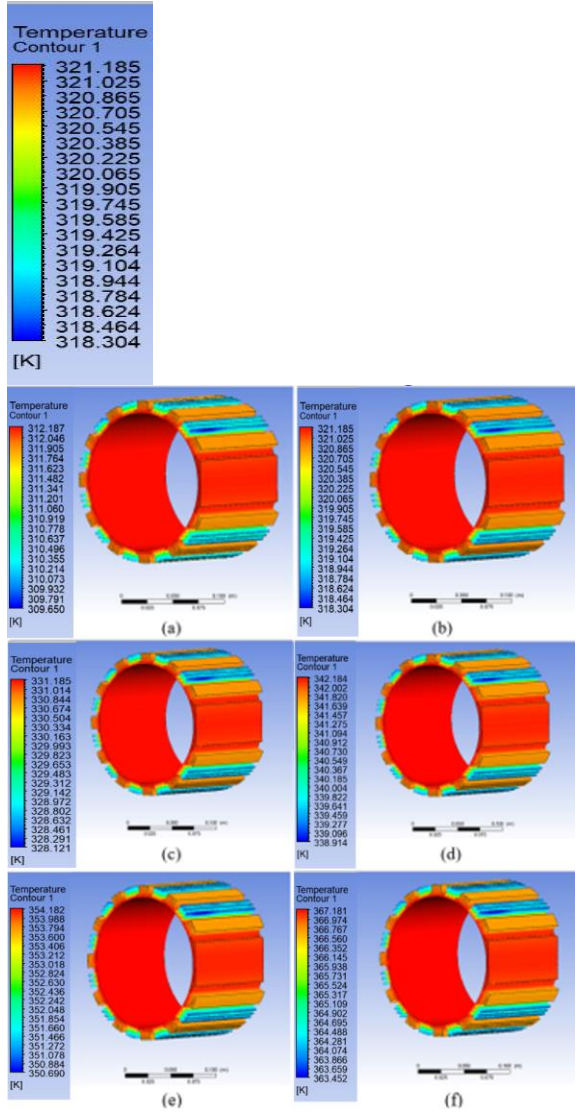


Fig. 6. CF heatsink standard motor simulation result; (a) winding motor temperature 39°C, (b) winding motor temperature 48°C, (c) winding motor temperature 58°C, (d) winding motor temperature 69°C, (e) winding motor temperature 81°C, and (f) winding motor temperature 94°C.

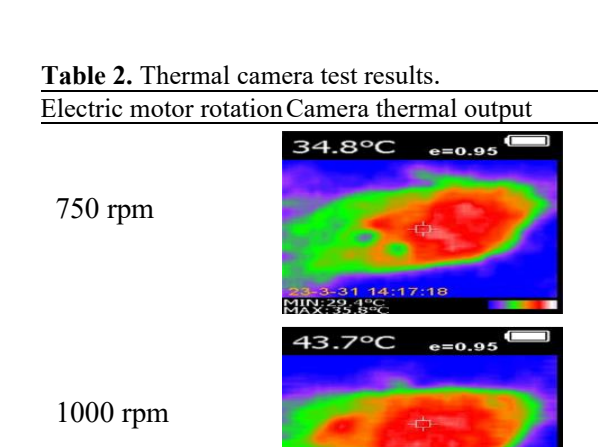


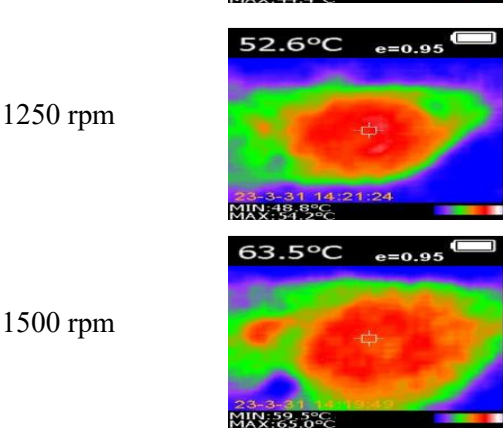
Fig. 7. Heatsink temperature at 750 rpm motor speed.

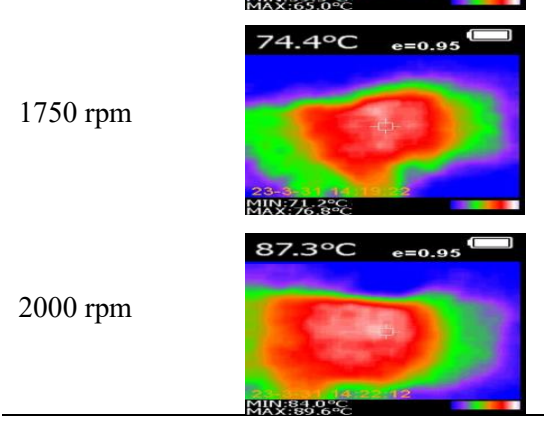
Table 3 provides the results of tests with different electric motor rotations using a thermal camera.

6. Result and discussion

Heatsink temperature simulation with winding temperature adjusted from the results of experimental research. Varying the winding temperature causes a difference in the value of heat distribution on the heatsink. The difference in the simulation results is depicted in Fig. 8. It shows the temperature change from the electric motor winding to the electric motor heatsink. At 750 rpm motor rotation and a winding temperature of 39°C, the temperature on the heatsink decreases to 34.8°C. At 1000 rpm motor rotation and a winding temperature of 48°C, the temperature on the heatsink becomes 58°C. At 1250 rpm motor rotation and a winding temperature of 58°C, the temperature on the heatsink decreases to 52.6°C. At 1500 rpm motor rotation and a winding temperature of 69°C, the temperature on the heatsink decreases to 63.5°C. At 1750 rpm motor rotation and a winding temperature of 81°C, the temperature on the heatsink decreases to 74.4°C.







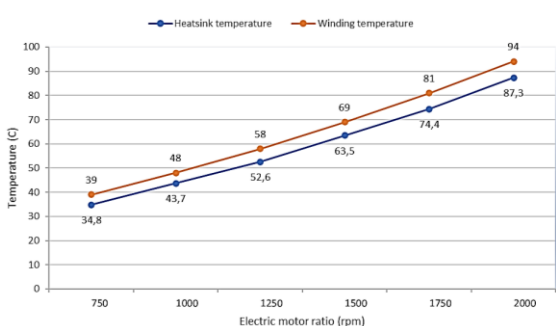


Fig. 8. Heatsink temperature simulation graph for the environment.

At a 2000 rpm motor rotation and a winding temperature of 94°C, the temperature on the heatsink drops to 87.3°C.

The temperature drop is still relatively small, so innovations are needed to make an optimal heatsink for this motorbike. The part that has a hot temperature is shown on the thicker outer part of the heatsink. Thus, it is necessary to make a few design changes so that the temperature distribution is more optimal. The heatsink simulation results above are used as data for simulating the effect of heatsink temperature on the environment. Assuming the vehicle speed is 38 km/h, the following is the difference from each simulation that has been carried out.

Fig. 9 shows the difference in the temperature simulation results that occur on the heatsink to the environment. At 750 rpm of electric motor rotation, the temperature value of the outside of the heatsink is 36.5°C, where heat transfer with the environment becomes 32.8°C. At 1000 rpm electric motor rotation, the temperature value of the outside of the heatsink is 45.1°C, heat transfer with the environment becomes 36.8°C. At low speed, the temperature transfer is less than at the higher motor speeds. Validation of the results from simulations and experiments is important for analysis because the suitability of the results indicates whether the simulation is

The cooling of electric motors tested by simulation and experiment is shown in Fig. 10. It compares the simulation (orange line) and experimental (blue line). It can be seen that there are differences in these results. At 750 rpm motor rotation, the simulation results show a heatsink temperature of 36.5°C, while the experimental results show 34.8°C.

valid or not.

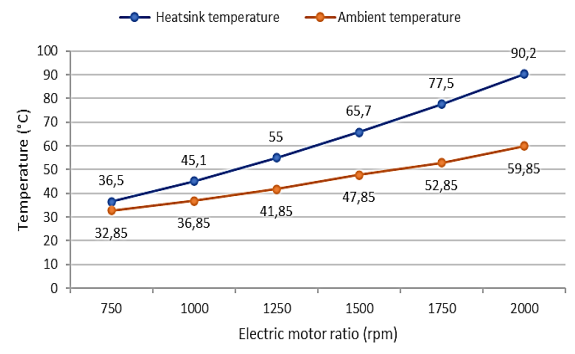


Fig. 9. Graph of heatsink temperature simulation on the environment.

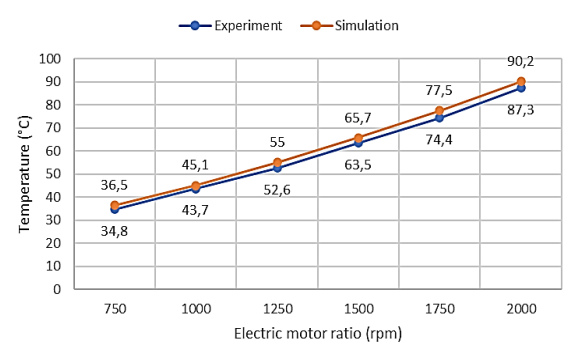


Fig. 10. Graph comparison of simulation and experiment results.

At 1000 rpm motor rotation, the simulation results show a heatsink temperature of 45.1°C, while the experimental results show a temperature of 43.7°C. At 1250 rpm motor rotation, the simulation results show a heatsink temperature of 55°C, while the experimental results show a temperature of 52.6°C. At 1500 rpm motor rotation, the simulation results show a heatsink temperature of 65.7°C, while the experimental results show a temperature of 63.5°C. At 1750 rpm motor rotation, the simulation results show a heatsink temperature of 77.5°C, while the experimental results show a temperature of 74.4°C. At 2000 rpm motor rotation, the simulation results show a heatsink temperature of 90.2°C, while the experimental results show a temperature of 87.3°C. The simulation and experimental results show a similar trend where the higher the rotation of the electric motor, the higher the heatsink temperature of the electric motor.

Research on "numerical and experimental study of a cooling of axial BLDC motor for electric scooter" shows that the temperature distribution in the cover casing is higher than that of the heatsink. These areas have lower effectiveness and need further cooling design attention. The simulation results using CFD are validated with experimental results. The simulation results can be used to evaluate the cooling of the axial BLDC motor. Winding temperature at a speed of 100 km/h is 105 °C with a magnetic temperature of 57.8 °C [17], whereas this research shows a trend similarity to that of the present study, which can be used to validate the simulation results. The maximum allowable simulation and experimental deviation value for the present

study is 5% [18-19]. With a deviation value below 5% and producing a similar trend of results, it can be concluded that the simulation results have been verified and can be declared valid. It can be seen from the values generated for temperature that the CFD simulation using Ansys Fluent software gives a higher value than the experimental results. The same thing was found in the CFD simulations that have been carried out, where the value of the CFD (fluid flow) simulation results is higher than the experimental value [20].

The mass loss per unit due to hysteresis, the eddy current in the stator yoke, and the eddy current in the stator tooth are calculated using Eq. (2) as:

Calculation:

o
$$Bm\beta = 1,21,6 \approx 1,339$$

o Per-kg hysteresis loss:

o fa = 1001 = 100

$$Ph = 0.01 \times 100 \times 1.339 = 1.34 \frac{W}{kg}$$

For 12 kg core $\rightarrow 1.34 \times 12 = 16.1 W$

To calculate the eddy current losses in the stator yoke can be calculated using Eq. (3):

0
$$K_h = 1.0 \times 10^{-4}$$

0 $f = 100 \, Hz$
0 $Bm = 1.2 \, T$
0 $\beta m = 0.20 \, m$
0 $r = 0.06 \, m$

Calculation:

$$P_{ey} = 1 \times 10^{-4} \times 8 \times \frac{100^2 \times 1.2^2}{0.20} \times 0.06^2.$$
 $P_{ey} = 0.0207 \ W$

The eddy current losses in the tooth stator can be calculated using Eq. (4):

$$P_{et} = 1.93 \, x \, 10^6 \, W \, (\approx 1.93 \, MW)$$

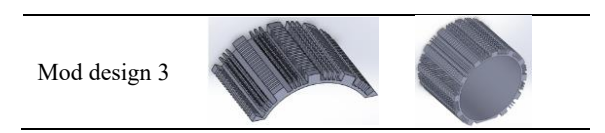
The following is the design proposed in this study after observing and analyzing the shape of the heatsink temperature distribution and heat transfer from the outside of the heatsink to the environment, shown in Table 3.

The change in temperature from the winding to the motor heatsink can be said to be very small. The change is 4°C. To increase the temperature transfer from the winding to the heatsink, it is necessary to make innovations to design electric motor heatsinks. So that the design can also affect the temperature changes that occur on the outside of the electric motor heatsink, depending on the surrounding environment. The design is determine temperature simulated to the distribution on the heatsink and to determine the heat transfer from the outside of the heatsink to the environment.

Table 3 is the latest heatsink design improvement after knowing the heatsink temperature point, which is still high. The original design of the electric motor is the default design of the motor, and no changes are made in this study. Mod design 1 is an electric motor design that is changed to a thick pin on the heatsink that comes with the electric motor.

Table 3. Heatsink design improvements.

Heatsink motor	Heatsink cutout design	Original heatsink design
Original design	ALLEN TO	
Mod design 1		
Mod design 2		



Mod design 2 is a design where pins are made radially to have a difference between the previous design, and also this design can transfer heat to the outside air faster than the axial shape, like the original design. Mod design 3 is a combination design of the shape of the axial and radial heatsink pins. The design change is expected to dissipate heat faster than the original design of the motor. The design is made based on the analysis obtained after obtaining the results of previous research. So that the temperature transfer from the heatsink to the surrounding environment is released more quickly when the electric motor is running. The design is simula ted to determine the temperature distribution on the heatsink.

The parameters of the meshing results using poly-hexcore type meshing in the old design are modified to 362278 cells, whereas in the new design, it is 420734 cells, and in the combination of old and new designs, it is 327877 cells, as shown in Fig. 11. In this new design, iterations are carried out until they converge. Graphs and convergence values from the simulation results are shown below. The convergence value of the residue generated from the modified old heatsink simulation is Energy = 9.4045e-07, in the new heatsink simulation is Energy = 9.8642e-07, and in the combination heatsink simulation is Energy = 9.6611e-07. The following is the result of a new heatsink simulation using Ansys Fluent software.

Table 4 is the result of a simulation of the electric motor heatsink redesign. The data used as a reference for determining the temperature of the winding motor are 39 °C, 48 °C, 58 °C, 69 °C, 81 °C, and 94 °C.

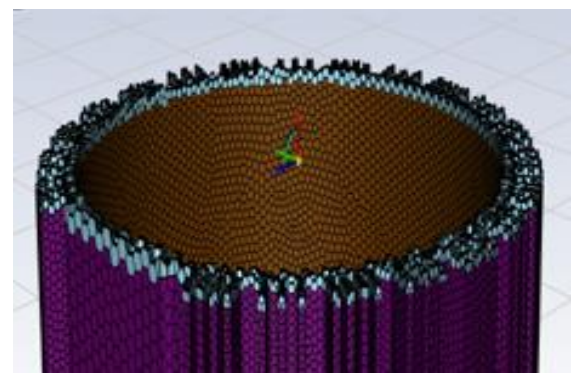


Fig. 11. Results of meshing redesigned heatsink.

Table 4. Simulation results of electric motor heatsink re-design

Original	Mod	Mod	Mod
design	design 1	design 2	design 3
Temperature Contour 1 312,187 312,186 313,206 313,206 313,206 311,764 311,624 311,482 311,482 311,080 310,778 310,778 310,778 310,778 310,355 310,214 310,355 310,214 310,355 310,214 310,355 310,214 310,355	Temperature Contour 1 312.052 311.816 311.380 311.347 310.875 310.875 310.898 300.666 309.689 309.453 308.272 308.208 308.272 308.208	Temperature Contour 1 311.973 311.973 311.618 310.828 310.523 310.168 310.523 310.169 309.435 309.472 308.772 308.772 307.7944 307.625 306.534 306.534 306.534 306.534	Temperature Contour 1 311.951 311.953 311.155 311.155 311.155 311.155 311.258 309.960 309.960 309.960 309.864 308.765 308.367 307.969 307.757 306.774 306.376 305.576 305.576
		Properties.	
		The second secon	
The second secon			

The data is also used in previous simulations obtained from experimental results. From the results obtained, there are differences in the results of the 3 designs above, and also differences with the standard electric motor heatsink design.

The comparison of the heatsink design simulation results in Fig. 12 is a comparison of the simulation results of the original and redesigned heatsink designs. It can be observed that there are differences in the results. At 750 rpm motor rotation, the original design results show a heatsink temperature of 36.5°C, whereas modif design 1 shows a heatsink temperature of 34.5°C, modif design 2 shows a heatsink temperature of 31.8°C, and modif design 3 shows a heatsink temperature of 31.5°C.

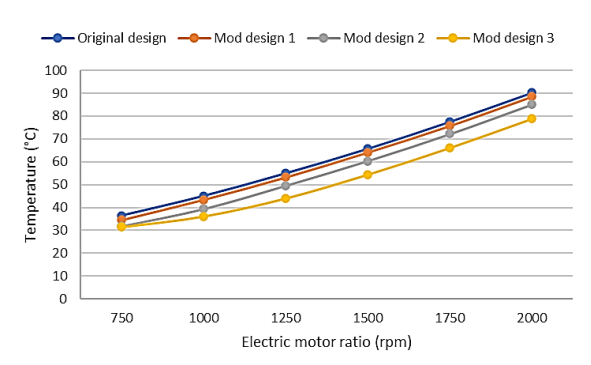


Fig. 12. Graph comparison of standard and redesigned heatsink design simulation results.

At 1000 rpm motor rotation, the results of the original design show a heatsink temperature of 45.1°C, while modif design 1 shows a heatsink temperature of 43.4°C, modif design 2 shows a heatsink temperature of 39.4°C, and modif design 3 shows a heatsink temperature of 36.2°C. At 1250 rpm motor speed, the original design results show a heatsink temperature of 55°C, whereas modif design 1 shows a heatsink temperature of 53.2°C, modif design 2 shows a heatsink temperature of 49.6°C, and modif design 3 shows a heatsink temperature of 44.1°C. At 1500 rpm motor rotation, the results of the original design show a heatsink temperature of 65.7°C, while modif design 1 shows a heatsink temperature of 64.1°C, modif design 2 shows a heatsink temperature of 60.4°C, and modif design 3 shows a heatsink temperature of 54.5°C. At 1750 rpm motor rotation, the original design results show a heatsink temperature of 77.5°C, whereas modif design 1 shows a heatsink temperature of 75.7°C, modif design 2 shows a heatsink temperature of 72.2°C, and modif design 3 shows a heatsink temperature of 66.2°C. At 2000

rpm motor rotation, the results of the original design show a heatsink temperature of 90.2°C, while modif design 1 shows a heatsink temperature of 88.5°C, modif design 2 shows a heatsink temperature of 85.1°C, and modif design 3 shows a heatsink temperature of 78.9°C.

From these data, it can be seen that design changes affect the temperature value of the heatsink, which is in line with the research of James Kuria and Pyung Hwang [21]. The latter believes that the effect of housing geometry is evaluated using three geometry designs, and the results show that the introduction of fins on the housing enhances heat transfer rate, and the end winding temperature can be reduced by up to 15%. Besides, the study from Sibi et al. [22] explains 3D CFD simulations performed in closed air on a fan-cooled brushless DC motor. As a heatsink, a package with fins is used, and with three heatsink designs, the different effects of fin shape on cooling performance are tested. The results show that at the ends of the coil, the highest temperature occurs, and by introducing a suitable cover, this temperature can be reduced by up to 15%. These results show that to improve the cooling performance of electric motors, CFD techniques can be used effectively. If seen from the temperature contour, it can be observed that the modif 2 heatsink design has the bluest temperature, but the value of the result is higher than the modif 3 heatsink design. Thus, the design that has the greatest heat transfer is modif 3. This is due to the design modif 3 has a larger cross-sectional area than modif 1 and 2. Modif 3 designs can have a greater heat transfer than the original heatsink design, modif 1 and modif 2. Changes in heat transfer occur as the electric motor rotates.

7. Conclusions

From the results and discussion of this study, several conclusions can be drawn:

1. The effect of motor rotation on the cooling of the BLDC motor heatsink becomes more pronounced as the motor rotation increases. Therefore, an increase in motor rotation can lead to higher temperatures in both the motor winding and heatsink.

- 2. The thermal distribution of BLDC motors can be analyzed using computational fluid dynamics (CFD) simulations on electric motor prototypes. This distribution begins with heat generation inside the heatsink and motor winding, followed by heat transfer to the outer heatsink of the electric motor.
- 3. Among the four BLDC motor cooling heatsink designs aimed at reducing the heatsink temperature of the largest BLDC motor, the modif 3 design, which combines radial and axial heatsink shapes, proves most effective. The temperature distribution in the modif 3 design achieves greater cooling compared to the original design and modifications 1 and 2. Consequently, the BLDC motor is less likely to experience overheating, excessive which could otherwise lead to reduced electric motor performance or even motor failure.

Acknowledgment

The authors are grateful to Poltrada Bali for technical support. The authors would also like to express their gratitude to Udayana University for supporting this research.

References

- [1] N. Anugrah, "Kementrian lingkungan hidup dan kehutanan gelar uji emisi tekan polusi udara di wilayah kota", *KLHK*, Jakarta, pp. 1, (2022).
- [2] M. Almaghrabi, Forced convection cooling of electric motors using enhanced surfaces, MSc Thesis, University of Central Florida, U.S.A., accessed in May (2016).
- [3] K. ESDM, "Peraturan menteri energi dan sumber daya mineral republik indonesia", *LL KESDM*, Jakarta, pp. 1-9, (2020).
- [4] W. Y. Perwira, N. S. Wardani and H. Bugis, "Effect of heatsink fin and thermal insulators on output of thermoelectric power of heat of motorcycle exhaust gas", *J. Mech. Eng. Vocat. Educ.*, Vol. 1, No. 2, pp. 5–8, (2018).
- [5] M. Mashadi and S. Purwanto, "Effect of magnetic properties in the addition of

- multiwalled carbon nanotube to material composite Fe0,8- C0,2", *J. Agric. Eng.*, Vol. 27, No. 3, pp. 175, (2012).
- [6] D. Montone, "Temperature effects on motor performance", *A.M.S.*, Pennsylvania, pp. 2–10, (2013).
- [7] Stekom, "Pembuang panas heatsink-basics", *W.B.M.*, Semarang, pp. 1, (2019).
- [8] J. Kuria and P. Hwang, "Investigation of thermal performance of electric vehicle BLDC motor", *Int. J. Mech. Eng.*, Vol. 1, No. 1, pp. 2277-7059, (2012).
- [9] D.T. Vu, and P. Hwang, "New cooling system design of BLDC motor for electric vehicle using computation fluid dynamics modeling", *J. Korean Soc. Tribol. Lubr. Eng.*, Vol. 29, No. 5, pp. 318–323, (2013).
- [10] M. Fasil, "Numerical and experimental investigation of heat flow in permanent magnet brushless DC hub motor", *SAE Int. J. Altern. Powertrains*, Vol. 4, No. 1, pp. 46–57, (2015).
- [11] J. Pyrhönen, "Heat-transfer improvements in an axial-flux permanent-magnet synchronous machine", *Appl. Therm. Eng.*, Vol. 76, No. 1, pp. 245-251, (2015).
- [12] A. Tikadar, "Parametric study of thermal performance of BMW I3", *Int. J. Mech. Prod. Eng.*, Vol. 8, No. 3, pp. 8–12, (2020).
- [13] Y. Wan, "Thermal analysis of a gramme-ring-winding high-speed permanent-magnet motor for pulsed alternator using CFD", *IET Electr. Power Appl.*, Vol. 14, No. 11, pp. 2111–2118, (2020).
- [14] K. Tarsisius, Marsono and S. Sayuti, "Liquid cooling model of axial BLDC motor", *J. Multidiscip. Eng. Sci. Studi.*, Vol. 6, No. 11, pp. 3569–3573, (2020).
- [15] M. E. Vakhshouri and B. Çuhadaroğlu, "A CFD analysis of the effects of injection and suction through a perforated square cylinder on some thermo-fluid parameters", J. Comput. Appl. Res. Mech. Eng. Vol. 11. No. 1,

pp. 23-33, (2021).

- [16] D.C. Ramesh, "Design and material optimization of cooling fins in electric motors", *Ann. Romanian Soc. Cell Biol.*, Vol. 25, No. 5, pp. 1991–2004, (2021).
- [17] A. Mukhlisin, "Study numerical and experimental a cooling of axial brushless direct current motor for electric scooter". *Proc. of 3rd Int. Conf. Mech. Eng.*, Vol. 1983, No. 1, pp. 3-8, (2018).
- [18] A. Workbench, "Ansys Fluent Tutorial Guide", 2nd ed., SAS IP Inc. Publisher, Canonsburg, U.S.A., (2017).
- [19] T. A. Dinham, C. Craddock, A. Lebas, and A. Ganguly, "Use of for hull form appendage design assessment on offshore patrol vessel and identification of wake focusing effect", R. Inst. Nav. Archit. Int. Conf., Southampton, Paper 1.
- [20] Y. Qi, and T. Ishihara, "Numerical study of turbulent flow around of a row of trees and an isolated building by using modified k-epsilon model and LES model", *J. Wind. Eng. Ind. Aerodyn.*, Vol. 177, No. 1, pp. 293-305, (2018).
- [21] J. Kuria and P. Hwang, "Optimizing heat sink geometry for electric vehicle BLDC motor using CFD", Sustain. Res. Innov. Conf. proc., Nairobi, Paper 19.
- [22] R. S. Sibi, A. N. Khaja and R. Rajeshkanna, "CFD simulation on cooling system of electric vehicle BLDC motor". *Int. Conf. Electr. Energy Syst.*, Chennai, Paper 22..